Journal of Alloys and Compounds 509 (2011) 1885–1892

Contents lists available at ScienceDirect

Journal of Alloys and Compounds

journal homepage: www.elsevier.com/locate/jallcom

Influence of $SrTiO_3$ nano-particles on the microstructure and shear strength of Sn–Ag–Cu solder on Au/Ni metallized Cu pads

Tama Fouzder[a], Ismathullakhan Shafiq[a], Y.C. Chan[a,*], A. Sharif[b], Winco K.C. Yung[c]

[a] Department of Electronic Engineering, City University of Hong Kong, Tat Chee Avenue, Kowloon Tong, Hong Kong
[b] Department of Materials and Metallurgical Engineering, Bangladesh University of Engineering and Technology, Dhaka 1000, Bangladesh
[c] Department of Industrial and Systems Engineering, The Hong Kong Polytechnic University, Hung Hom, Kowloon, Hong Kong

ARTICLE INFO

Article history:
Received 4 July 2010
Received in revised form 11 October 2010
Accepted 21 October 2010
Available online 30 October 2010

Keywords:
Nano doping
Ball grid array solder joints
Shearing force
Microstructure

ABSTRACT

Nano-sized, nonreacting, noncoarsening $SrTiO_3$ particles have been incorporated into Sn–3.0 wt% Ag–0.5 wt% Cu solder alloys and the interfacial microstructure and the shear strength on Au/Ni metallized Cu pads ball grid array substrates investigated as a function of the number of reflow cycles and aging time. At their interfaces, a scallop-shaped ternary Sn–Ni–Cu intermetallic compound layer was found in both plain Sn–Ag–Cu solder joints and solder joints containing $SrTiO_3$ nano-particles, and the intermetallic compound layer thickness increased with the number of reflow cycles and aging time. After the addition of $SrTiO_3$ nano-particles, in the solder ball region, a fine microstructure of $AuSn_4$, Ag_3Sn, Cu_6Sn_5 intermetallic compounds appeared in the β-Sn matrix. In addition, the shear strength of solder joints containing $SrTiO_3$ nano-particles exhibited a consistently higher value than that of plain Sn–Ag–Cu solder joints due to a second phase dispersion strengthening mechanism as well as a refinement of the intermetallic compounds. The fracture surface of plain Sn–Ag–Cu solder joints exhibited a brittle fracture mode with a smooth surface while Sn–Ag–Cu solder joints containing $SrTiO_3$ nano-particles showed ductile failure characteristics with rough dimpled surfaces.

1. Introduction

Many regulations have been introduced over the world to urge the elimination of lead and lead-containing solders, due to increasing pressure by the environmental and health concerns associated with lead-containing solders in the electronics industry. Owing to the realization of the inherent toxicity of lead (Pb) and lead-containing alloys on the environment and human health, increasing efforts have been made to search for suitable lead-free solders as replacement for the conventional Sn–Pb eutectic alloy [1–4]. Thus, many research groups are concerned with the development of new lead-free solders and their composites. Up to now, several types of binary and ternary Sn-based Pb-free solder systems have been discussed in the literature including Sn–Bi, Sn–Zn, Sn–Zn–Bi, Sn–Ag, Sn–Ag–Zn, Sn–Zn–In, Sn–Bi–Ag and Sn–Ag–Cu [5–7]. Among the numerous lead-free solders, ternary Sn–Ag–Cu solder alloys, with near eutectic compositions and melting temperatures of around 217 °C, are regarded as promising candidates to replace the traditional Sn–Pb solder for application in the electronic packaging industry [8,9]. However, due to rapid formation of brittle intermetallic compound layers at the solder and substrate interface, the reliability of these solder joints has been a serious concern [10]. In addition, Anderson et al. [11] reported that the formation of large primary dendrite-shaped β-Sn grains in Sn–Ag–Cu solder retarded the resistance to thermal–mechanical fatigue.

With the advancement of micro-/nanosystems technology towards a higher speed, smaller, thinner and portable features, an increasing quest for better performance and continual miniaturization as well as reliability, the electronic packaging industry especially when applying ball grid array packages and flip chips are facing severe limitations [12]. In general, the reliability of solder joints is greatly influenced by the interfacial reactions between the substrate and solder, the difference in coefficients of thermal expansion, elastic modulus, shear strength, fatigue and creep behavior [13]. During a reflow process, intermetallic compound (IMC) layers are formed inevitably at the interface between the solder and substrate. Moreover, due to solid-state diffusion, the IMC layer becomes thicker and thicker with more reflow cycles and thermal aging stages [14]. The properties of solder joints as well as the reliability of the whole package are very sensitive to the thickness and morphology of the IMC layers at the interfaces of the joints. Although the formation of an IMC layer is important for good wetting and bonding, an excessively thick layer is harmful because of its brittle nature which

* Corresponding author. Tel.: +852 27887130, fax: +852 2788 7579.
E-mail address: eeycchan@cityu.edu.hk (Y.C. Chan).

0925-8388/$ – see front matter © 2010 Elsevier B.V. All rights reserved.
doi:10.1016/j.jallcom.2010.10.081

makes it prone to mechanical failure even under a low load [15].

Studies have shown that one innovative, potentially viable and economically affordable approach, to stabilize a fine grain microstructure and give homogeneous deformation of solder joints as well as to improve the mechanical properties of a solder, is the addition of an appropriate secondary phase to a solder matrix to form a composite solder. A survey of the literature showed that micro/nano-sized particles of alloying elements such as silver, copper, nickel, antimony and bismuth improved the mechanical properties of a lead-free solder while simultaneously reducing the melting point [16–18]. In addition, various nano-sized, nonreacting, noncoarsening oxide dispersoids have been incorporated into solder alloys to create a new, improved solder structure which exhibits significantly enhanced creep resistance combined with increased strength [19]. Shen and Chan [20] successfully prepared a ZrO_2 reinforced composite solder by mechanically dispersing ZrO_2 nano-particles into a eutectic Sn–9Zn solder paste and this composite solder had a much improved shear strength. Noh et al. [21] used Ce particles as reinforcements for a conventional Sn–Ag solder and reported significant enhancement in wettability and mechanical properties. Tai et al. [22] prepared 20 vol.% Cu_6Sn_5 reinforced Sn–3.5Ag composite solder by an in situ method and the composite solder joint exhibited a better steady-state creep strain rate, less thermomechanical fatigue damage and higher shear strengths after different numbers of thermomechanical fatigue cycles as compared to a plain Sn–3.5Ag solder joint. Recently, Tsao and Chang [23] developed a series of Sn–3.5Ag–0.25Cu composite solders reinforced with different weight percentages (0, 0.25, 0.5 and 1 wt%) of TiO_2 nano-particles and measured their mechanical properties. Among them, a Sn–3.5Ag–0.25Cu composite solder containing 1 wt% TiO_2 nano-particles showed significant improvements in the yield strength, microhardness and ultimate tensile strength. In the current study, strontium titanate ($SrTiO_3$) particles of a nanometer size were used. The main advantages of $SrTiO_3$ nano-particles are: (a) a similar density to Sn–Ag–Cu, ρ(Sn–3.5Ag–0.5Cu) = 7.11 and $\rho(SrTiO_3) = 5.12\,g/cm^3$ as compared to other ceramic particles such as $\rho\,(Al_2O_3) = 3.97\,g/cm^3$, $\rho(TiO_2) = 3.89\,g/cm^3$, and (b) a higher hardness as compared to a Sn–3.5Ag–0.5Cu matrix.

However, the result of a literature search revealed that no studies have been made so far to develop lead-free Sn–Ag–Cu composite solders containing $SrTiO_3$ nano-particles. Accordingly, the aim of the present study is to prepare lead-free Sn–Ag–Cu composite solders with 0.5 wt% $SrTiO_3$ nano-particles. In addition, plain and composite solders were characterized for their interfacial microstructures and shear strengths on Au/Ni metallized Cu pads as a function of the number of reflow cycles and aging time.

2. Experimental procedures

Composite solders were prepared primarily by mechanically dispersing 0.5 wt% $SrTiO_3$ nano-particles into the Sn–3.0Ag–0.5Cu (AMTECH, USA) solder powder. The mixtures were blended manually for at least 30 min to create a uniform distribution of the $SrTiO_3$ nano-particles with a water-soluble flux (Qualitek Singapore (PTE) Ltd.). Then, the paste mixture was printed onto alumina substrates using a stainless steel stencil with a thickness of 0.15 mm and reflowed in a reflow oven (BTU International, Pyramax-100N) at 250 °C to prepare solder balls about 0.76 mm in diameter.

A solder mask-defined copper bond pad on a flexible substrate of a ball grid array (BGA) package was used as a base for the electrodeposition of Ni and Au. The solder mask-opening diameter was 0.6 mm with a 7 μm thick Ni layer deposited on the ball pad. The average thickness of the Au layer was 0.5 μm. Lead-free solder balls with a diameter of 0.76 mm, were placed on prefluxed Au/Ni/Cu bond pads of the substrates and reflowed at a temperature of 250 °C with a belt speed of 70 cm min^{-1} in a convection reflow oven (BTU International, Pyramax-100N). After the reflow process, the samples were cooled to room temperature and cleaned with isopropyl alcohol (IPA). Then, the assembled packages were aged isothermally at 150 °C for 10–40 days in a high temperature oven to examine the interfacial reactions between the solder and substrate. Then, to characterize the microstructures, the reflowed and aged samples were cross-sectioned and mounted in a resin, then ground by different grit sizes of emery papers and polished with an 0.5 μm Al_2O_3 suspension and etched with 5% dilute HCl. Finally, the interfacial morphology at the solder alloy/BGA substrate interface was observed using a scanning electron microscope (SEM, Philips XL 40 FEG) with the backscattered electron (BSE) imaging mode and an energy dispersive X-ray spectrometer (EDX, International, model no. DX-4) was utilized to determine the chemical composition of the IMCs. The accuracy of the compositional measurements was typically ±5%. To find out the formula composition of the IMCs, the chemical analyses of the EDX spectra were corrected by standard atomic number, absorption, fluorescence (ZAF) software. Before SEM observations, the samples were sputter coated with Au to avoid effects due to charging. Transmission electron microscopy (TEM, JEOL JEM 2100F) was used for the observation of the $SrTiO_3$ nano-particles.

The melting characteristics of the plain Sn–Ag–Cu solder and the Sn–Ag–Cu–0.5 wt% $SrTiO_3$ composite solder were investigated using a differential scanning calorimeter (DSC Q 10). For the DSC analysis, 10 mg of each solder was placed into an aluminum pan and scanned from 100 °C to 275 °C at a rate of 10 °C min^{-1} under a nitrogen atmosphere. X-ray diffraction (XRD, Philips PW 3040 X'Pert PRO) was used to determine the crystalline phase of the $SrTiO_3$ nano-particles contained in the composite solder.

To measure the shear strength, ball shear tests were performed on the reflowed and aged samples using a shear testing machine (PTR-1000, Rhesca Co. Ltd., Japan) with a 50 μm shear tool height and 500 μm/s shear speed. The average strength of twenty solder balls with the minimum and maximum values removed was taken for each condition. After ball shear testing, the fracture surfaces and compositions were investigated thoroughly using SEM and EDX techniques.

3. Results and discussion

Fig. 1(a and b) shows bright field TEM images of $SrTiO_3$ nano-particles and (c) a selected area diffraction pattern of $SrTiO_3$ nano-particles. In the TEM images, spherically shaped $SrTiO_3$ nano-particles, about 90–110 nm, in diameter were clearly observed. In the low magnification TEM observation (Fig. 1(a)), it seems the nano-particles inside one cluster were in contact. However, when the sample was tilted and observed at a higher magnification, there were often some spaces between the particles as shown in Fig. 1(b).

Fig. 2 shows the DSC results of (a) plain Sn–Ag–Cu solder and (b) solder containing 0.5 wt% $SrTiO_3$ nano-particles. From the DSC results, the melting temperatures of plain Sn–Ag–Cu solder and the solder containing $SrTiO_3$ nano-particles were about 217 °C and 217.7 °C, respectively, with only a eutectic peak. There was an elevation of the melting temperature of less than 1 °C for the Sn–Ag–Cu composite solder doped with $SrTiO_3$ nano-particles. From the DSC profiles, it was clear that it was not necessary to change the existing solder process parameters such as the reflow temperature when applying the Sn–Ag–Cu-0.5$SrTiO_3$ composite solder.

Fig. 3 shows XRD profiles of (a) $SrTiO_2$ nano-particles and (b) Sn–Ag–Cu solder doped with 0.5 wt% $SrTiO_3$ nano-particles. From XRD profile (a), it was clear that $SrTiO_3$ nano-particles appeared as a crystalline phase with sharp peaks. On the other hand, in the composite solder alloy in the XRD profile (b), Ag_3Sn, Cu_6Sn_5 intermetallic compounds and the $SrTiO_3$ phase were easily detected as well as the β-Sn phase. It is well known that the dissolved Ag and Cu will precipitate by forming Ag_3Sn and Cu_6Sn_5 intermetallic compounds in the solder matrix during solidification [24].

Fig. 4 shows the backscattered scanning electron micrographs of (a, c and e) plain Sn–Ag–Cu solder and (b, d and f) solder joints containing 0.5 wt% $SrTiO_3$ nano-particles depending on the number of reflow cycles at 250 °C which were taken at the interfaces between the solder and Au/Ni metallized Cu pads. At their interfaces, a ternary scallop-shaped Sn–Ni–Cu intermetallic compound layer was clearly observed with a dark contrast in both plain solder joints and solder joints containing $SrTiO_3$ nano-particles. Yoon et al. [25] noted that there is a small atomic size difference between Cu and Ni, and since both have the same FCC lattice structure, the substitution of Ni into Cu_6Sn_5, without causing a lattice distortion or the formation of a new phase, was reasonable. It can be seen that the outer very thin entire Au layer (0.5 μm) in the Au/Ni metallized Cu pads ball grid array has dissolved into the molten solder and $AuSn_4$ was formed within the bulk Sn–Ag–Cu solder. Therefore, no

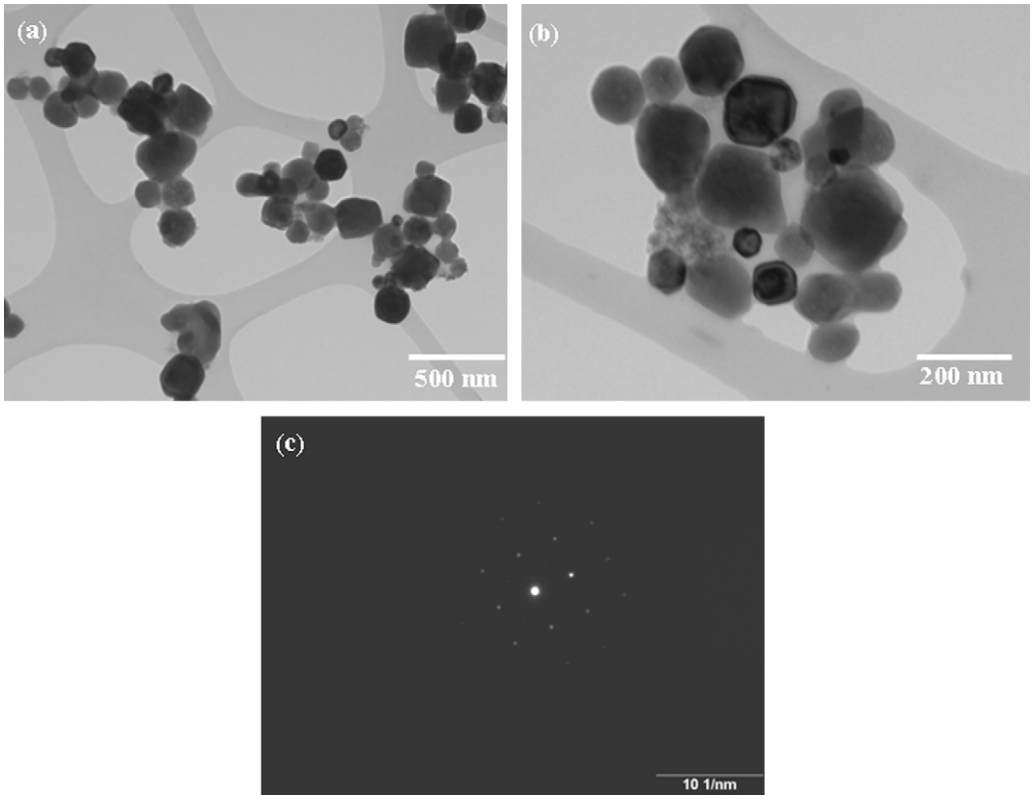

Fig. 1. Bright field TEM images (a and b) and selected area diffraction pattern (c) of $SrTiO_3$ nano-particles.

Au-containing intermetallic compound or Au layer was found at the interface. In addition, with an increase in the number of reflow cycles the scallop-shaped Sn–Ni–Cu intermetallic compound layer thickness was substantially increased in both solder joints. However, after the addition of $SrTiO_3$ nano-particles, the scallop-shaped Sn–Ni–Cu intermetallic compound layer growth rate was relatively lower than that in a plain Sn–Ag–Cu solder joint. The reason may be that the second phase $SrTiO_3$ nano-particles change the driving force for the growth of the intermetallic compound layer as well as the diffusivity of the elements involved in its growth. Li et al. [26] reported that rare earth elements reduce the rate of formation of the intermetallic compound layer in two ways i.e. by changing the diffusion coefficient and thermodynamic parameters of the elemental affinity.

Fig. 5 shows backscattered scanning electron micrographs of (a and c) a plain Sn–Ag–Cu solder joint and (b and d) a solder joint containing 0.5 wt% $SrTiO_3$ nano-particles as a function of the number of reflow cycles at 250 °C which were taken from the solder ball regions. After one reflow cycle, in the solder ball region needle-shaped Ag_3Sn, spherical-shaped Cu_6Sn_5 and $AuSn_4$ intermetallic compounds were clearly observed in a β-Sn matrix. The plausible

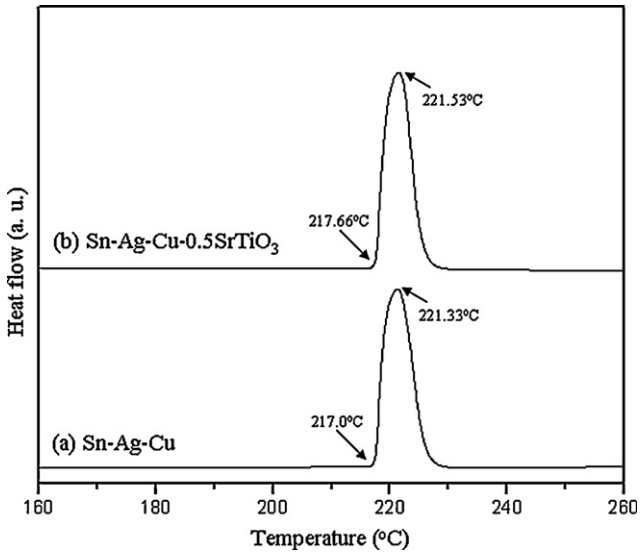

Fig. 2. DSC profiles of (a) plain Sn–Ag–Cu and (b) Sn–Ag–Cu–0.5$SrTiO_3$ composite solder alloys.

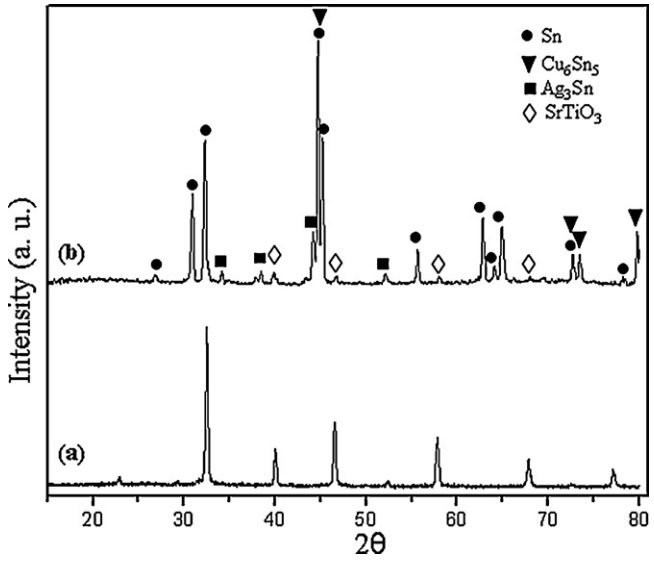

Fig. 3. XRD profiles of (a) $SrTiO_3$ nano-particles and (b) Sn–Ag–Cu–0.5$SrTiO_3$ composite solder alloy.

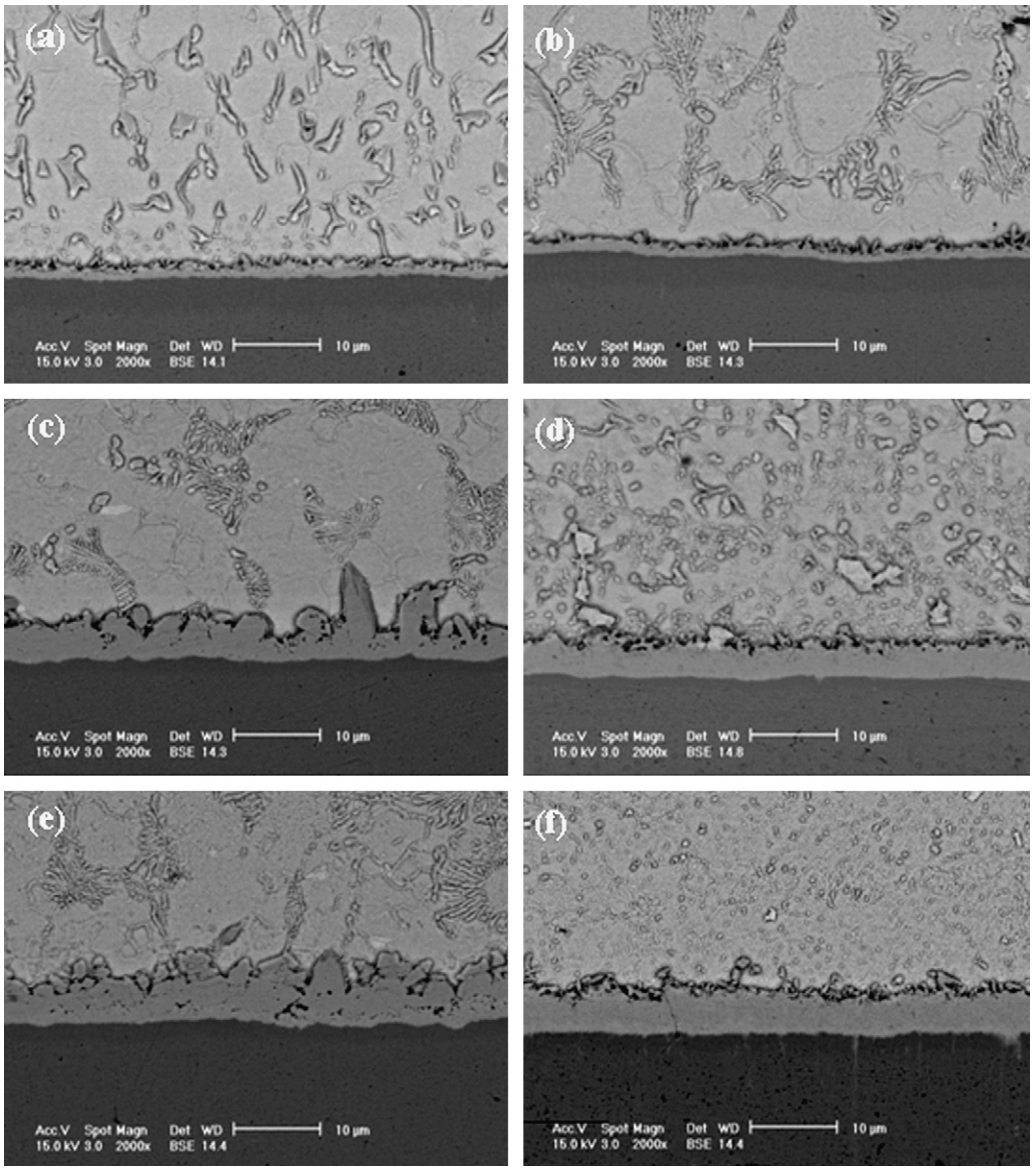

Fig. 4. SEM micrographs of (a, c and e) plain Sn–Ag–Cu solder and (b, d and f) Sn–Ag–Cu–0.5$SrTiO_3$ composite solder joints after (a and b) one, (c and d) eight and (e and f) sixteen reflow cycles (interfacial regions).

explanation here is that the formation of the $AuSn_4$ intermetallic compound in the solder ball region is due to the dissolution of the Au layer from the Au/Ni metallized Cu pads on the BGA substrate. The $AuSn_4$ phase was found only as scattered particles in the microstructure and no type of $AuSn_4$ layer segregation next to the intermetallic layers was observed. However, after the addition of $SrTiO_3$ nano-particles, needle-shaped Ag_3Sn, spherical-shaped Cu_6Sn_5 and $AuSn_4$ intermetallic compounds were found as well as a substantial decrease in the β-Sn grain size which appeared with a fine microstructure. The dendrite-shaped β-Sn grain size after one reflow cycle of a plain Sn–Ag–Cu solder joint was about 10–15 μm while the grain size of a Sn–Ag–Cu–0.5$SrTiO_3$ solder joint was about 7–10 μm. However, with an increase in the number of reflow cycles from one to eight, the needle-shaped Ag_3Sn, spherical-shaped Cu_6Sn_5 and $AuSn_4$ intermetallic compounds as well as the β-Sn grain size were significantly increased in plain Sn–Ag–Cu solder joints as compared with solder joints containing $SrTiO_3$ nano-particles. The reason may be that the second phase reinforcing $SrTiO_3$ nano-particles promote a high nucleation density in the eutectic colonies during solidification. From this result, it is clear that the second phase $SrTiO_3$ nano-particles retarded the growth rate of intermetallic compounds.

Fig. 6 shows backscattered scanning electron micrographs of interfacial regions (a and c) Sn–Ag–Cu solder joints and (b and d) Sn–Ag–Cu–0.5$SrTiO_3$ composite solder joints as a function of aging time i.e. (a and b) after 10 days aging and (c and d) after 40 days aging at 150 °C. It is clear that the Sn–Ni–Cu intermetallic compound layer thickness increased substantially with an increase in the aging time in Sn–Ag–Cu solders joints and solder joints containing 0.5 wt % $SrTiO_3$ nano-particles. However, the scallop-shaped Sn–Ni–Cu intermetallic compound layer growth rate in a plain Sn–Ag–Cu solder joint was faster than that of a composite solder joint as shown in Fig. 6.

Fig. 7 shows backscattered scanning electron micrographs of (a and c) plain Sn–Ag–Cu solder joints and (b and d) solder joints containing 0.5 wt% $SrTiO_3$ nano-particles as a function of aging time i.e. (a and b) after 10 days and (c and d) after 40 days aging at 150 °C which were taken from the solder ball region. Ag_3Sn and Cu_6Sn_5 as well as $AuSn_4$ intermetallic compounds were clearly observed in the β-Sn matrix in both plain Sn–Ag–Cu solder joints and composite

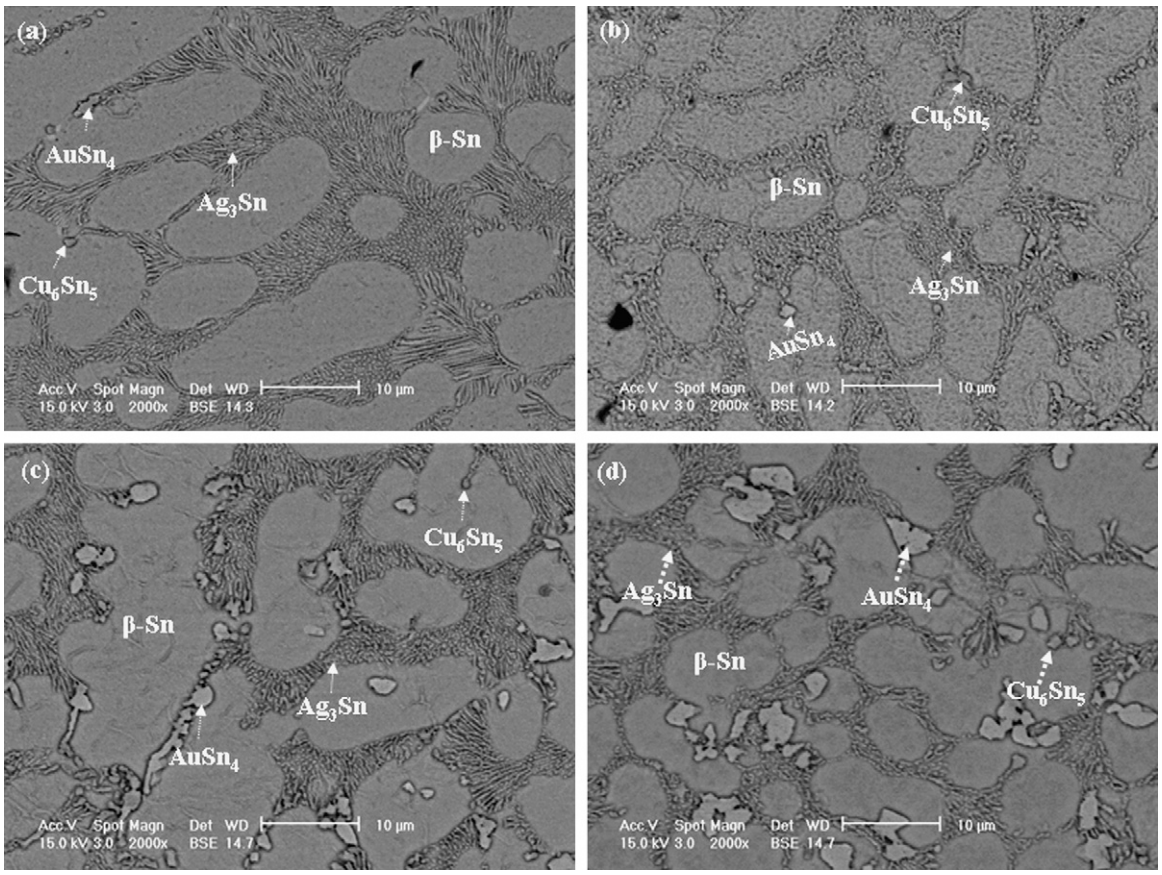

Fig. 5. SEM micrographs of (a and c) plain Sn–Ag–Cu solder and (b and d) Sn–Ag–Cu–0.5$SrTiO_3$ composite solder joints after (a and b) one and (c and d) eight reflow cycles (solder ball regions).

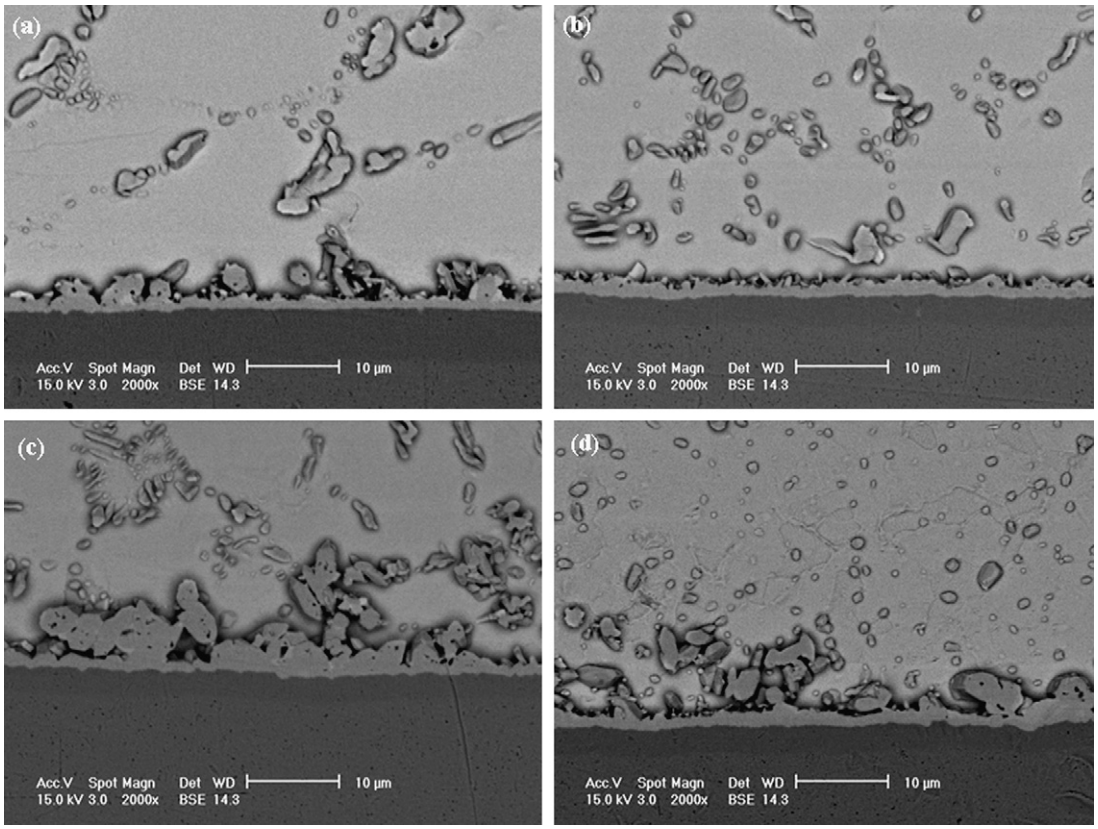

Fig. 6. SEM micrographs of (a and c) plain Sn–Ag–Cu solder and (b and d) Sn–Ag–Cu–0.5 $SrTiO_3$ composite solder joints after aging (a and b) 10 days and (c and d) 40 days at 150 °C (interfacial regions).

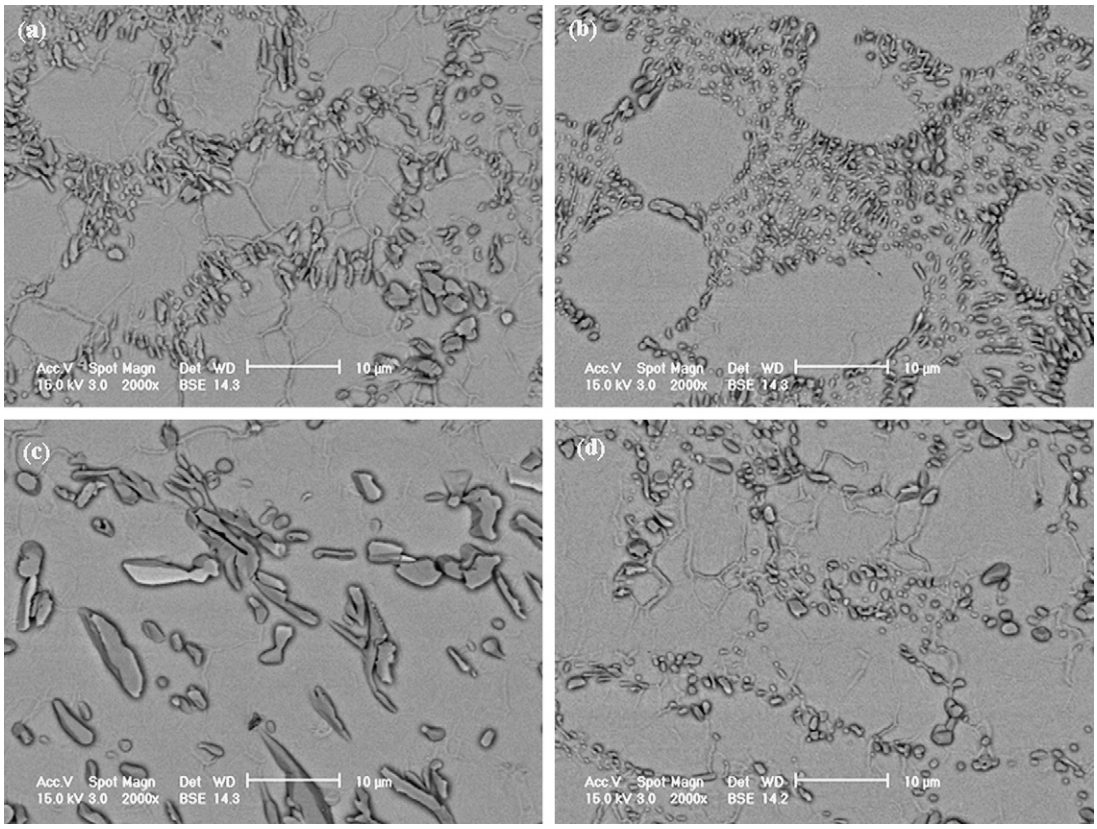

Fig. 7. SEM micrographs of (a and c) plain Sn–Ag–Cu solder and (b and d) Sn–Ag–Cu–0.5$SrTiO_3$ composite solder joints after aging (a and b) 10 days and (c and d) 40 days at 150 °C (solder ball regions).

solder joints. However, after the addition of $SrTiO_3$ nano-particles, the sizes of the Ag_3Sn, Cu_6Sn_5 and $AuSn_4$ intermetallic compounds were greatly decreased to become finer particles as shown in Fig. 7(b and d). A plausible explanation here for the finer intermetallic compound particles is the absorption of $SrTiO_3$ nano-particles with a high surface free energy on the grains during solidification. In addition, the eutectic phase further spread to form network areas after the addition of $SrTiO_3$ nano-particles as shown in Fig. 7(a and b).

Fig. 8 plots the variation of intermetallic compound layer thickness of plain Sn–Ag–Cu solder joints and solder joints containing 0.5 wt% $SrTiO_3$ nano-particles as a function of the number of reflow cycles. The average thickness of the intermetallic compound layer was calculated by using the following equation: $T = (t_1 + t_2 + t_3 + \ldots + t_n)/n$ where $t_1, t_2, t_3, \ldots t_n$ are the thicknesses of the intermetallic compound layer at various positions on the interface. It may be seen that the intermetallic compound layer thickness of all solder joints increased with an increase in the number of reflow cycles. The IMC layer thicknesses of plain Sn–Ag–Cu solder joints and solder joints containing 0.5 wt% $SrTiO_3$ nano-particles after one reflow cycle were about 2.1 μm and 1.7 μm, respectively, while their IMC thicknesses after sixteen reflow cycles were about 6.7 μm and 5.8 μm, respectively. From this result, it is clear that the $SrTiO_3$ nano-particles retarded the growth of the intermetallic compound layer.

Since solder joints are often subjected to mechanical loading during processing and system use, the mechanical properties of solder joints, such as their shear strength is crucial to their reliability. Therefore, ball shear tests were performed to evaluate the effect of the interfacial reactions on the mechanical reliability of Sn–Ag–Cu–0.5$SrTiO_3$ composite solder joints on Au/Ni metallized Cu pad BGA substrates as a function of the number of reflow cycles

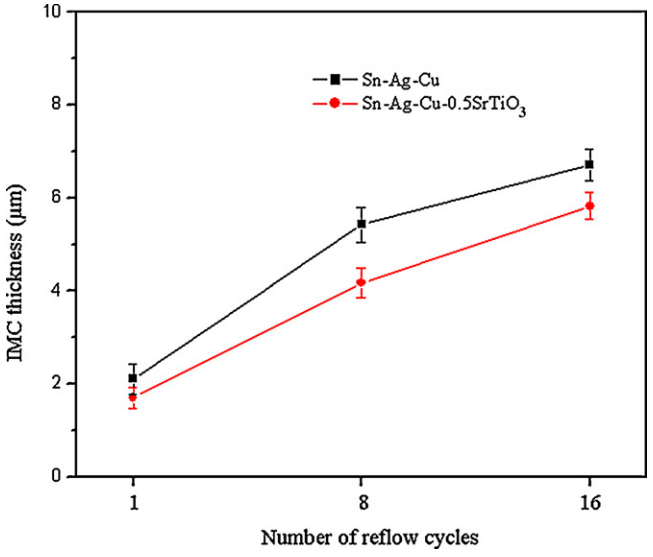

Fig. 8. IMC layer thickness of plain Sn–Ag–Cu solder and Sn–Ag–Cu–0.5$SrTiO_3$ composite solder joints as a function of the number of reflow cycles.

and aging time. Fig. 9 shows the variation of the ball shear strength of plain Sn–Ag–Cu solder and Sn–Ag–Cu–0.5$SrTiO_3$ composite solder joints as a function of the number of reflow cycles (a) and aging time (b). The shear strengths of plain Sn–Ag–Cu solder joints after one reflow cycle and sixteen reflow cycles were about 38 and 31.6 MPa, respectively. On the whole, the shear strength of solder joints containing $SrTiO_3$ nano-particles changed very little as a function of the number of reflow cycles and aging time due to the

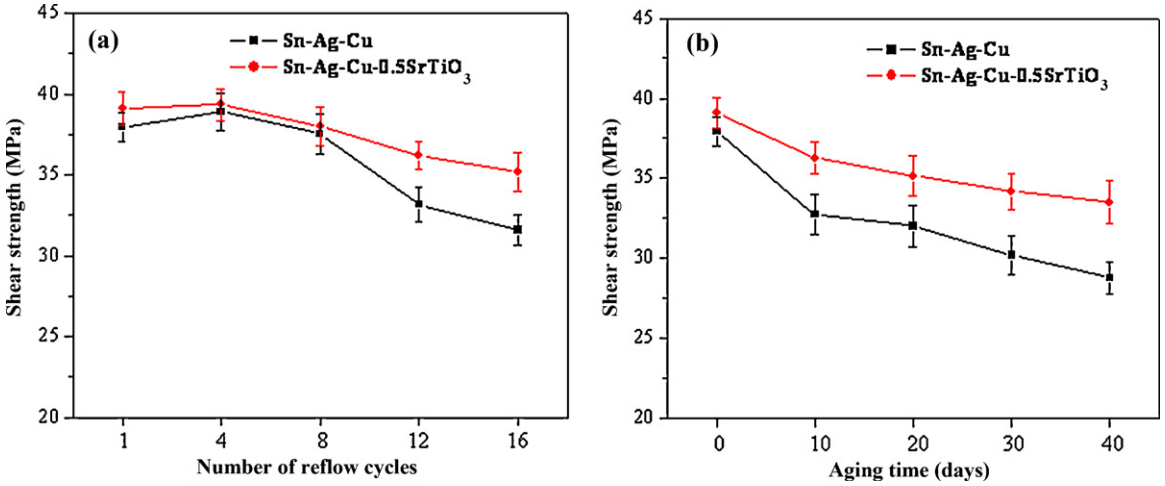

Fig. 9. Shear strength of plain Sn–Ag–Cu solder and Sn–Ag–Cu–0.5$SrTiO_3$ composite solder joints as a (a) function of the number of reflow cycles and (b) aging time.

homogeneous distribution of $SrTiO_3$ nano-particles as well as the well-controlled fine microstructure. However, the composite solder joints consistently displayed a higher shear strength than that of the plain Sn–Ag–Cu solder joints for each number of reflow cycles and aging time. A plausible explanation here for the higher shear strength is due to the well-controlled intermetallic compound layer as well as the refinement of the Cu_6Sn_5, Ag_3Sn, $AuSn_4$ intermetallic compounds and the $SrTiO_3$ nano-particles dispersed throughout the β-Sn matrix. In addition, according to a dispersion strengthening mechanism, the fine intermetallic compounds and $SrTiO_3$ nano-particles improve the mechanical properties of the solder joint. This can be attributed to (1) pinning grain boundaries, (2) being obstacles to the movement of dislocations and increased dislocation densities and (3) a strengthening mechanism of the matrix, from the finely dispersed intermetallic compounds and $SrTiO_3$ nano-particles [27]. The shear strengths of Sn–Ag–Cu–0.5$SrTiO_3$ solder joints after one reflow cycle and sixteen reflow cycles were about 39.1 MPa and 35.3 MPa, respectively. On the other hand, after aging at 150 °C for 40 days, the shear strength value of plain Sn–Ag–Cu solder joints and solder joints containing 0.5 wt% $SrTiO_3$

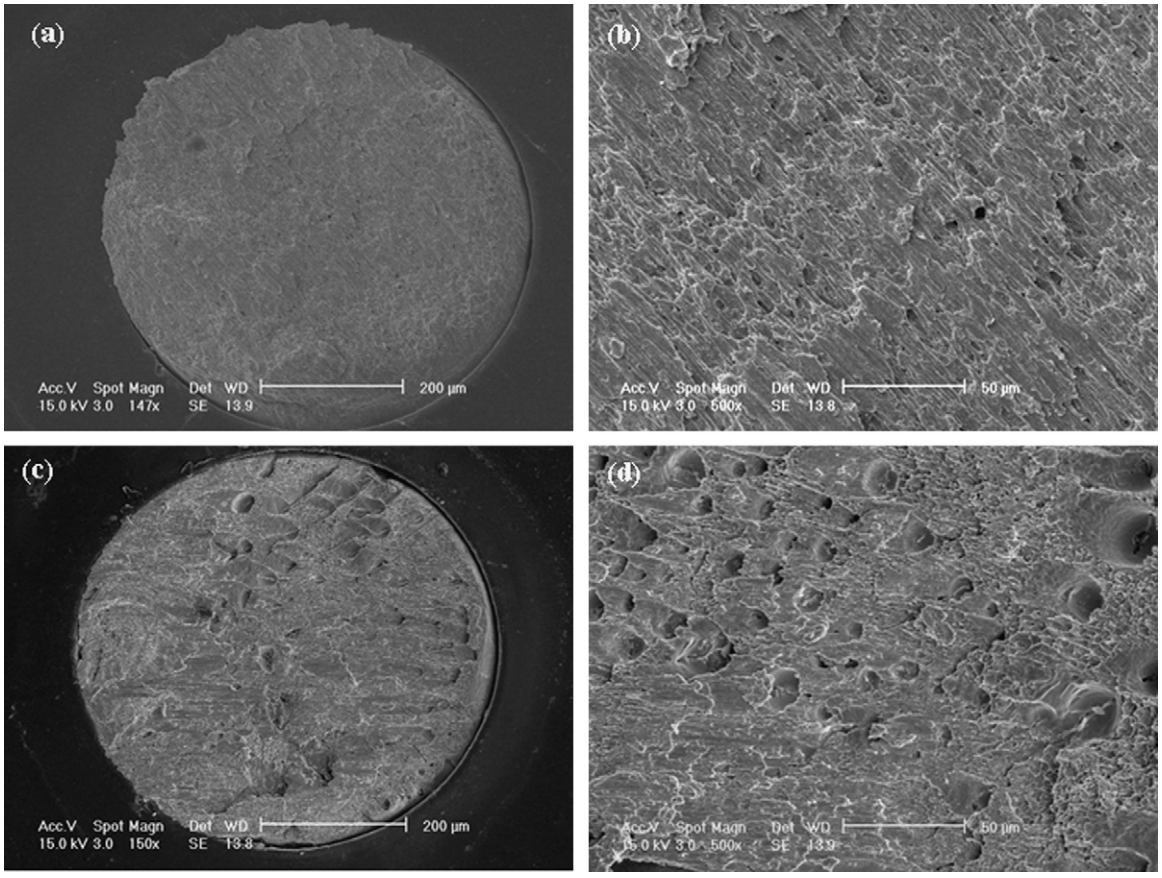

Fig. 10. SEM micrographs of fracture surfaces of (a and b) plain Sn–Ag–Cu solder and (c and d) Sn–Ag–Cu–0.5$SrTiO_3$ composite solder joints after one reflow cycle.

nano-particles were about 28.8 MPa and 33.5 MPa, respectively. After aging at a high temperature (150 °C) for 40 days the shear strength of a composite solder joint did not change significantly due to the homogeneous distribution of $SrTiO_3$ nano-particles as well as the refined microstructure of intermetallic compound particles in the solder matrix.

To verify the variations of the shear strength found in the ball shear test, the fracture surfaces after the ball shear tests were examined using SEM and are presented in Fig. 10. In the plain Sn–Ag–Cu solder joints after one reflow cycle (Fig. 10(a and b)), the fracture surface exhibited a brittle fracture mode with a relatively smooth surface. By contrast, Sn–Ag–Cu solder joints containing $SrTiO_3$ nano-particles showed ductile failure with very homogeneous dimpled surfaces as shown in Fig. 10(c and d) due to the homogeneous distribution of $SrTiO_3$ nano-particles.

4. Conclusions

In the present study, the effect of $SrTiO_3$ nano-particles on the interfacial reactions, the morphology of IMC and the shear strength between solder joints and Au/Ni metallized Cu pads were investigated as a function of reflow cycles and aging time. At the interface, a scallop-shaped ternary Sn–Ni–Cu intermetallic compound layer was found in both plain Sn–Ag–Cu solder and composite solder joints. Also the intermetallic compound layer thickness was substantially increased with an increase in the number of reflow cycles and aging time. In addition, needle-shaped Ag_3Sn, spherical-shaped Cu_6Sn_5 and $AuSn_4$ intermetallic compound particles were clearly observed in the β-Sn matrix in the solder ball region. However, after the addition of $SrTiO_3$ nano-particles, these intermetallic compounds appeared in a finer dispersion due to the high nucleation density and high surface free energy on the grain surface promoted by the $SrTiO_3$ nano-particles in the eutectic solder during solidification.

The Sn–Ag–Cu–0.5$SrTiO_3$ composite solder joints consistently displayed higher shear strengths than that of the plain Sn–Ag–Cu solder joints for each number of reflow cycles due to a second phase dispersion strengthening mechanism as well as a controlled fine dispersion of intermetallic compound particles. In addition, the solder joints containing $SrTiO_3$ nano-particles gave a ductile fracture with a very rough surface due to the uniform distribution of $SrTiO_3$ nano-particles.

Acknowledgements

The authors acknowledge the financial support provided by City University of Hong Kong for the project 9041222 CERG grant of Hong Kong Research Grants Council and RGC ref. no. 111307 (development of a nano-activator doped surface modifier for Sn-Zn based lead-free soldering). Professor Brian Ralph at Brunel University is thanked for proof reading the manuscript.

References

[1] S.E. Negm, H. Mady, A.A. Bahgat, J. Alloys Compd. 503 (2010) 65–70.
[2] A.K. Gain, T. Fouzder, Y.C. Chan, A. Sharif, W.K.C. Yung, J. Alloys Compd. 489 (2010) 678–684.
[3] H. Tsukamoto, T. Nishimura, S. Suenaga, K. Nogita, Mater. Sci. Eng. B 171 (2010) 162–171.
[4] S.H. Wang, T.S. Chin, C.F. Yang, S.W. Chen, C.T. Chuang, J. Alloys Compd. 497 (2010) 428–431.
[5] C.Y. Lin, U.S. Mohanty, J.H. Chou, J. Alloys Compd. 501 (2010) 204–210.
[6] A.K. Gain, Y.C. Chan, A. Sharif, W.K.C. Yung, Microelectron. Eng. 86 (2009) 2347–2353.
[7] K. Kanlayasiri, M. Mongkolwongrojn, T. Ariga, J. Alloys Compd. 485 (2009) 225–230.
[8] F. Cheng, F. Gao, H. Nishikawa, T. Takemoto, J. Alloys Compd. 472 (2009) 110–115.
[9] W.M. Xiao, Y.W. Shi, G.C. Xu, R. Ren, F. Guo, Z.D. Xia, Y.P. Lei, J. Alloys Compd. 472 (2009) 198–202.
[10] H.B. Kang, J.H. Bae, J.W. Lee, M.H. Park, Y.C. Lee, J.W. Yoon, S.B. Jung, C.W. Yang, Scripta Mater. 60 (2009) 257–260.
[11] I.E. Anderson, J.C. Foley, B.A. Cook, J. Harringa, R.L. Terpstra, O. Unal, J. Electron. Mater. 30 (2001) 1050–1059.
[12] J. Shen, Y.C. Chan, J. Alloys Compd. 477 (2009) 909–914.
[13] M. Ahmed, T. Fouzder, A. Sharif, A.K. Gain, Y.C. Chan, Microelectron. Reliab. 50 (2010) 1134–1141.
[14] P. Liu, P. Yao, J. Liu, J. Alloys Compd. 470 (2009) 188–194.
[15] Y.Y. Shiue, T.H. Chuang, J. Alloys Compd. 504 (2010) 610–617.
[16] A.K. Gain, Y.C. Chan, W.K.C. Yung, Mater. Sci. Eng. B 162 (2009) 92–98.
[17] Y.W. Wang, Y.W. Lin, C.T. Tu, C.R. Kao, J. Alloys Compd. 478 (2009) 121–127.
[18] A.K. Gain, T. Fouzder, Y.C. Chan, A. Sharif, N.B. Wong, W.K.C. Yung, J. Alloys Compd. 506 (2010) 216–223.
[19] L.C. Tsao, S.Y. Chang, C.I. Lee, W.H. Sun, C.H. Huang, Mater. Des. 31 (2010) 4831–4835.
[20] J. Shen, Y.C. Chan, J. Alloys Compd. 477 (2009) 552–559.
[21] B.I. Noh, J.H. Choi, J.W. Yoon, S.B. Jung, J. Alloys Compd. 499 (2010) 154–159.
[22] F. Tai, F. Guo, M.T. Han, Z.D. Xia, Y.P. Lei, Y.W. Shi, Mater. Sci. Eng. A 527 (2010) 3335–3342.
[23] L.C. Tsao, S.Y. Chang, Mater. Des. 31 (2010) 990–993.
[24] X. Liu, M. Huang, Y. Zhao, C.M.L. Wu, L. Wang, J. Alloys Compd. 492 (2010) 433–438.
[25] J.W. Yoon, S.W. Kim, S.B. Jung, J. Alloys Compd. 392 (2005) 247–253.
[26] B. Li, Y. Shi, Y. Lei, F. Guo, Z. Xia, B. Zong, J. Electron. Mater. 34 (3) (2005) 217–224.
[27] Y. Shi, J. Liu, Z. Xia, Y. Lei, F. Guo, X. Li, J. Mater. Sci.: Mater. Electron. 19 (2008) 349–356.